Journal of Atmospheric and Solar–Terrestrial Physics 208 (2020) 105384

Contents lists available at ScienceDirect

Journal of Atmospheric and Solar–Terrestrial Physics

journal homepage: www.elsevier.com/locate/jastp

Research paper

Small-scale structures in noctilucent clouds observed by lidar

Britta Schäfer [a,b,*], Gerd Baumgarten [a], Jens Fiedler [a]

[a] Leibniz-Institute of Atmospheric Physics at the Rostock University, Schlossstraße 6, 18225 Kühlungsborn, Germany
[b] University of Oslo, Postbox 1022, Blindern, 0315 Oslo, Norway

ARTICLE INFO

Keywords:
Noctilucent clouds
Small-scale structures
Lidar
Gravity waves

ABSTRACT

Noctilucent clouds (NLC) are mesospheric ice clouds occurring in the summer hemisphere at high latitudes and an altitude of about 83 km. This region is the coldest of the earth's atmosphere and is characterized by the presence of wave interaction and dissipation. The processes involved here lead to a variety of structures and instabilities that become visible in noctilucent clouds and are observed by different instruments. In this work high-resolution lidar measurements are used to give a wide overview of the structures at small scales below the Brunt–Väisälä period of ~5 min. For the first time a large amount of NLC profiles from lidar with a temporal resolution of 1 s is analyzed in detail, covering about 1400 h during the summer from 2011 to 2018. A new categorization focusing on small-scale structures is introduced, and occurrence statistics for these categories in the season of 2014 are performed. Both wave structures with periods below 10 min and thin layers of < 100 m thickness are commonly found. When taking simultaneous wind measurements into account, we find that structures often are advected by the wind.

1. Introduction

Observations of noctilucent clouds (NLC) were for the first time reported in 1885 independently by three scientists in different European countries. These were Otto Jesse in Steglitz (Berlin, Germany), Robert C. Leslie in Southampton (England) and Thomas W. Backhouse in Kissingen (Bavaria, Germany) (Jesse, 1885; Leslie, 1885; Backhouse, 1885). It is very likely that these initial observations were triggered by the eruption of Krakatoa in 1883, even though ice particles in the mesosphere might have existed before that time (Lübken et al., 2018). As supposed by Thomas et al. (1989) the anomalously large amount of water vapor ejected into the stratosphere by this event might also have led to an increased transport of H_2O into the mesosphere, making the growth of ice particles possible that are big enough to be seen from the earth's surface. The second requirement for NLC formation apart from the presence of water vapor is a sufficiently low temperature which applies to the summer mesosphere due to the reversed seasonal cycle in temperature at these altitudes compared to the surface. This seasonal cycle is gravity-wave driven and minimum temperature values during summer are 130 K and below (Lübken, 1999).

Beside their own attributes like occurrence frequency and spatial spread, noctilucent clouds include other features that make them very relevant for atmospheric research. They are a unique tracer to visualize middle atmosphere dynamics and it is still a current research subject to which extent NLC particles can be seen as inert tracers. This is the case when the ice particles stay invariant in terms of size through relevant time scales. Measurement and model results regarding formation time, particle size, growth and density have been discussed extensively (e.g., Karlsson and Rapp, 2006; Kiliani et al., 2013; Turco et al., 1982; Zasetsky et al., 2009). Particles with radius larger than about 20 nm are big enough to be detected by optical measurement techniques, maximum sizes reach about 70 nm. Smaller particles of a few nanometer yield radar echoes called Polar Mesospheric Summer Echoes (PMSE) that often occur simultaneously with NLC in the middle atmosphere and lower thermosphere (Nussbaumer et al., 1996; Kaifler et al., 2011). In terms of dynamics this region is characterized by the dissipation of energy and momentum due to the breaking of upward propagating waves transporting energy and momentum from the surface to higher layers. Most prominent among them are gravity waves with buoyancy as their restoring force. To conserve kinetic energy, their amplitudes increase along with the decrease in air density when propagating upwards, until the waves begin to dissipate and break and finally convert into turbulence. Then they create a variety of structures that are observed in NLC by many means: (1) naked eye, (2) camera, (3) lidar profiles, (4) in-situ measurements on rockets, (5) high-resolution satellite measurements. For NLC structures in camera images categories have been described as morphology types by Fogle and Haurwitz (1966). A similar categorization for lidar data has not been performed so far, but is relevant because, when measuring the smallest scales in NLC, lidars are the most powerful instruments providing both high resolution and long

* Corresponding author at: University of Oslo, Postbox 1022, Blindern, 0315 Oslo, Norway.
E-mail address: britta.schafer@geo.uio.no (B. Schäfer).

https://doi.org/10.1016/j.jastp.2020.105384
Received 30 March 2020; Received in revised form 2 July 2020; Accepted 6 July 2020
Available online 10 July 2020

time series. Previous research by Kaifler et al. (2013) and Ridder et al. (2017) has emphasized the presence of wave signatures down to very small scales. Even though the waves observed here are by far too small in scale (a few km) to be directly resolved in atmospheric circulation models, they are represented by parametrizations. In order to make this representation as reliable as possible, it is important to improve our knowledge about small-scale waves from observations. Ridder et al. (2017) used a pattern recognition technique calculating the match between a generalized structure template and the observed feature, where the shortest templates were of 5 min duration with a sampling interval of 30 s. Kaifler et al. (2013) focused on datasets with the same resolution, but also showed one example of a single-shot acquisition measurement with subsecond temporal resolution (i.e. recording the received photons for every single laser shot individually). Another example is published by Fritts et al. (2017). Both expose structures that have not been resolved by measurements before and in order to understand these phenomena, an analysis of a larger amount of this highest-resolution data has to be performed.

The following article addresses this issue through a descriptive treatment of the smallest scales found in NLC. For the first time a large amount of lidar data with 1 s temporal and 25 m range resolution from the years 2011 to 2018 is analyzed in a systematic way. The structure of the paper is as follows: In chapter 2 the instruments, used in this study, are introduced. In the data analysis in chapter 3, a new categorization for NLC types, based on lidar data, is introduced and in chapter 4 their occurrence statistics are performed throughout the summer 2014.

2. Instruments

2.1. ALOMAR RMR lidar

The instrument providing the data for this research is the RMR lidar located at the Arctic Lidar Observatory for Middle Atmosphere Research (ALOMAR) in Northern Norway at 69° N, 16° E. It is operated on routine basis throughout the whole year and optimized for NLC detections during summer. This double lidar system uses two injection-seeded Nd:YAG lasers with a wavelength of 1064 nm and its second and third harmonics at 532 nm and 355 nm as emitters and two steerable telescopes of 1.8 m diameter as receivers. During the seasons contributing to this work the repetition frequency was 30 Hz with an averaged power of ~14 W per laser (Baumgarten, 2010). A detailed description of the system is given by von Zahn et al. (2000), and updates concerning NLC detection between 1994 and 2017 are listed in Fiedler et al. (2017). In the described setting, daytime lidar measurements are possible for altitudes up to 90 km. The daylight capability makes the ALOMAR RMR lidar the only lidar in the world that can measure noctilucent clouds during the whole summer at polar latitudes with high time resolution.

Since the first NLC detection with the ALOMAR RMR lidar in 1994 many improvements have been added to the system leading to a higher resolution of the data. Since 2011 a lidar single-shot acquisition system (LISA) has been installed at ALOMAR yielding a temporal resolution of 33 ms and a range resolution of 25 m. The database to study small-scale structures from that is huge and covers approximately 1400 h of NLC measurements from 2011 to 2018. In this work, for the first time a large number of events comprising the whole season 2014 and strong NLC events from the other years is analyzed in detail. While all three wavelengths emitted by the lidar are important, for example for NLC particle size measurements as well as other applications than NLC, in noctilucent cloud studies with LISA only the 532 nm channel is used, because it is the most sensitive concerning NLC detection. The brightness of an NLC is determined by the backscatter from the ice particles, and therefore the aerosol backscatter coefficient β_a is used to describe NLC in lidar data. From the raw signal (counts per time interval and range bin) this property is derived by taking the ratio of total ($\beta_v = \beta_a + \beta_m$) to molecular backscatter β_m, where the latter is calculated from the MSISE-00 model (Picone et al., 2002). Further on, the background is removed by subtracting the averaged signal from above the NLC and, β_v is normalized with respect to the value in the altitude range of 45–50 km, where no aerosols are expected, i.e. $\beta_v = \beta_m$. Finally, the aerosol backscatter coefficient is calculated as $\beta_a(z) = \beta_v(z) - \beta_m(z)$ where z is the altitude. In this way, influences from variations in the lower atmosphere or in the laser power are eliminated from the measurement results. In the following figures, β_a is also termed as β_{532} indicating the wavelength. A more detailed description of this method is given by Baumgarten et al. (2007).

2.2. Meteor radars

Horizontal neutral winds at NLC altitudes have been obtained from combining radial velocities from two closely located specular meteor radars, i.e., Andenes (16.04°E, 69.27°N), and Tromsø (19.22°E, 69.58°N). Details of each system can be found in Singer et al. (2004) and Hall et al. (2005), respectively. The combination of measurements from these two radars not only allows more counts and therefore better temporal and altitudinal resolutions than each of the systems individually, but more importantly allows the estimation of horizontal wind gradients. These gradients can in turn be combined to get horizontal divergence and relative vorticity (Chau et al., 2017). In this work we have used estimations obtained with 2 km and 1 h vertical and temporal resolutions, respectively.

3. Data analysis

3.1. Data set

The lidar data from the single-shot acquisition system spans the seasons from 2011 until 2018. Since the ALOMAR RMR lidar is a twin lidar there are two records from the same time during most of the measurements. Typical pointings of the lidar beams are in vertical direction (zenith) and tilted 20° off-zenith in northern (system 1) and eastern direction (system 2). When tilted, the spatial separation between the two observed volumes at NLC altitudes is about 40 km. In this case, the two NLC volumes generally show big differences concerning internal small-scale structures, so the measurements can be treated as independent of each other for the analysis focusing on small scales.

3.2. Categorization of small-scale features in high-resolution lidar data

The investigation of small-scale structures in noctilucent clouds has already been addressed by different studies as Ridder et al. (2017) and Kaifler et al. (2013). Nevertheless, the term “small-scale” has to be defined every time it is used since essential innovations have led to even higher resolutions than ever before and therefore enabled the detection of structures down to scales that have not been observable previously. Already in 2017, studies were performed where a 2D-pattern recognition was applied to identify wave structures in NLC data with 30 s resolution (Ridder et al., 2017). The templates used in this method represented general structure patterns of NLC altitude variations in time due to waves. Compared to the resolution of 10 min typically used by other lidar instruments, new features were found and described. Here the usage of the single-shot acquisition system LISA makes it possible for us to resolve wave signatures, instabilities and mixing processes in NLC on scales below one minute and a few hundred meters. Fig. 1 shows a comparison of this data with data of 30 s resolution on the same date. It becomes clear that segments in the 30 s data that expose discontinuities (jumps) become continuous in higher resolved data by uncovering structures on shorter periods. Looking into the data with 1 s resolution uncovers so many different and individual patterns that it is currently no longer meaningful to apply a similar pattern recognition technique as Ridder et al. (2017) on time scales below five minutes. Instead, a characterization of the events is made

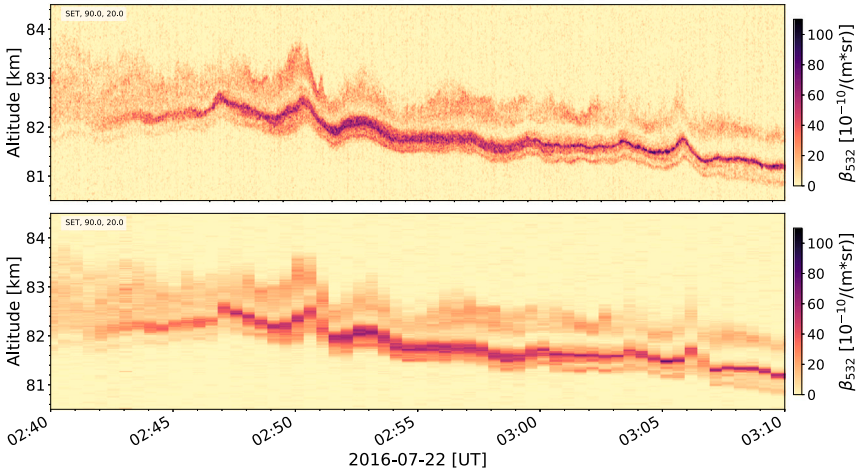

Fig. 1. NLC backscatter coefficient in ALOMAR lidar data from July 22, 2016, 02:40 - 03:10 [UT]: The upper panel has a resolution of 1 s from the single-shot acquisition system, the lower picture shows the same data integrated for 30 s. The name and pointing of the telescope are given in the upper left corner, where the first number is the azimuth and the second is the zenith distance angle. The color scale represents the NLC backscatter coefficient at 532 nm β_{532} in 10^{-10}/(m sr).

individually and new categories are defined and assigned to them. In the style of types for NLC structures in images defined by Fogle and Haurwitz (1966), the following categorization to identify patterns in NLC focusing on vertical structure and the occurrence of instabilities is proposed:

I. Thin layers (<500 m)
   (a) Smooth up and down drift, wave periods > 10 min, associated with unperturbed waves.
   (b) Short period height variations (<10 min), either short period waves or irregular height variations.

II. Layers of middle thickness (0.5–1 km)
   (a) Smooth up and down drift, wave periods > 10 min, associated with unperturbed waves.
   (b) Short period height variations (<10 min), either short period waves or irregular height variations:
      i. Constant vertical backscatter profile throughout the layer.
      ii. Higher backscatter at the upper or lower edge of the layer.

III. Thick layers (> 1 km)
   (a) Smooth up and down drift, wave periods > 10 min, no explicit multi-layer composition:
      i. Constant vertical backscatter profile throughout the layer.
      ii. Higher backscatter at the upper or lower edge of the layer.
   (b) Irregular structure in time and range (thickness of the layer may vary with changing substructure, containing periodic structures on time scales < 10 min).
   (c) Multi-layer composition:
      i. Parallel movement of the layers.
      ii. Non-parallel movement of layers, including creation and extinction when entering or leaving a certain height region.

We refer to the division after thickness (I, II, III) as "types" and name their subdivisions "categories", examples are given in Figs. 2–6. These measurements have been selected after screening the lidar data from 2011 to 2018, and they represent the typical structures of interest categorized above. We have looked through the dataset via inspecting multiple one-hour lengths of time series similar to Figs. 2–6, as this timespan allows us to see the small scale structures and their larger-scale environment. The definition of the categories is mainly based on empiricism reflecting the visual sensation of the structures. The differentiation starts with separating NLC layers by thickness since the vertical range, in which the background conditions are suitable for NLC to occur, is the first and foremost condition to consider during any particular NLC event. Type III is divided into more categories than type I since a thicker layer can involve a lot more phenomena inside. Short-period structures are addressed in all three NLC types by the categories I b, II b, and III b. Additionally, category III b is a pool to collect cases that cannot be assigned to another group due to the presence of many structure types at the same time.

In categories II b and III a, the differentiation between a constant vertical backscatter coefficient profile throughout the layer (i.) and a higher brightness at the lower or upper edges of the layer (ii.) is made in order to account for the variety of wave activities causing particle growth and sublimation. Upward winds and corresponding cold phases of waves enable high supersaturation and particle growth to visible sizes, while downward motions lead to adiabatic warming of the particles and make them disappear quickly (Kiliani et al., 2013). As the lifecycle of NLC particles is dominated by sedimentation, one typically expects the largest particles, and therefore the highest brightness, at the bottom of the layer, right before they vanish. Other stratifications in NLC may indicate contributions of processes or background conditions other than the described ones.

In Fig. 2 a layer of category I a is shown, i.e. a thin layer not exposing short period altitude variations, but embedded in a larger-scale wave. The next Fig. 3 shows an example of category I b with altitude variations on remarkably short time scales. The backscatter does not change with altitude indicating that these times are too short to be subject to changes in particle size. Fig. 4 is the first one to show two simultaneously recorded profiles of different NLC volumes. It reveals that the small-scale structure differs significantly in volumes with a horizontal separation of 40 km. The following Figs. 5–7 are recorded in the same setup. Fig. 5 shows the categories II b i and III a i

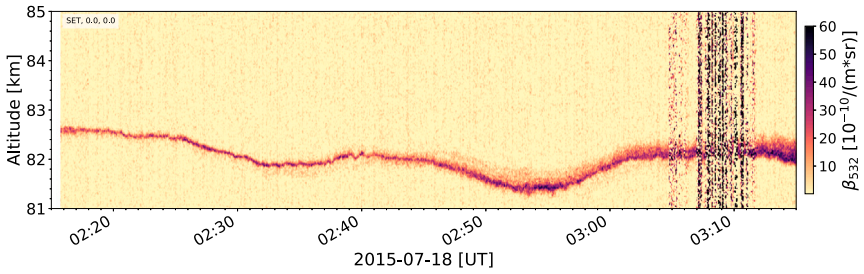

Fig. 2. NLC time-height section for one hour of measurements on July 18, 2015 showing a layer of category I a. The text in the upper left corner indicates the name of the telescope and its pointing (azimuth, zenith distance angle). Times with low signal to noise ratio appear as vertical lines with a dark shaded pattern. Both systems were viewing in zenith direction and measuring the same NLC, therefore only one system is shown.

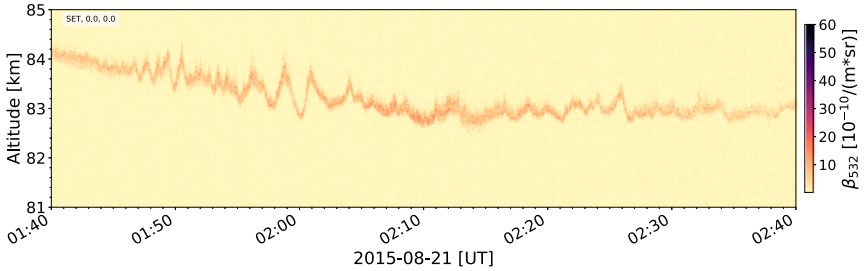

Fig. 3. NLC on August 21, 2015 showing a layer of category I b. Both systems were viewing in zenith direction and giving the same result, only one is shown.

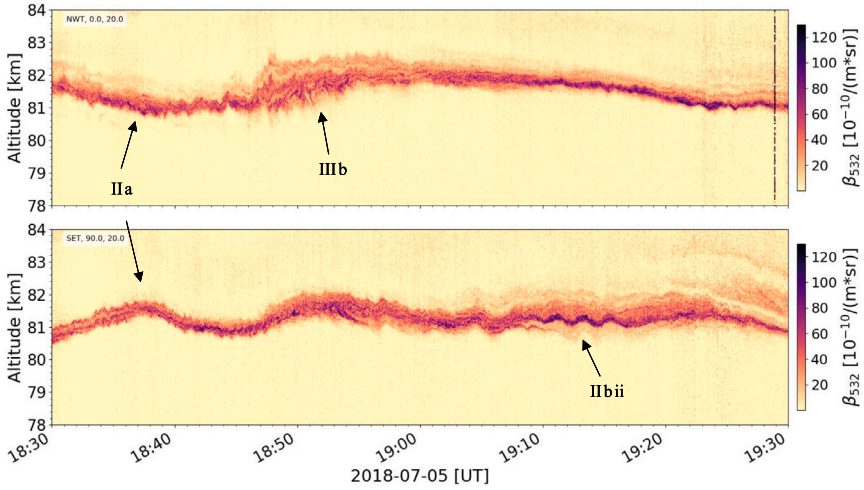

Fig. 4. Simultaneous observation of NLC in two sounding volumes, separated by about 40 km on July 05, 2018 showing the categories II a, II b ii and III b as labeled. Here the two telescopes were pointing 20° off-zenith towards North (upper panel) and East (lower panel). In the II b ii region, the backscatter is stronger at the lower edge of the layer.

for a case in which the NLC vanishes earlier in the second volume (measured by system 2) than in the first. In Fig. 6 resembling category III a ii, the visual differences between both volumes are smaller than in Fig. 5 although the spatial separation of the measurement volumes is the same. Fig. 7 shows one example for the variety of structures that are covered by category III b. It contains both very thin layers (<100 m) and very short period altitude variations (<1 min). As the last example, Fig. 8 shows up to five parallel moving layers as described in category III c i with narrow vertical separations down to ~100 m of width for each.

4. Results and discussion

4.1. Occurrence statistics

Since the total amount of data recorded by the single-shot acquisition system is very large and the categorization has to be performed manually, in this preliminary study we have reduced the data volume by extracting subsets. One season is a reasonable choice for that and the year 2014 is selected due to the longest duration of total NLC detection throughout this year. The total measurement duration of the NLC season in 2014 was 417 h, whereof during 270 h noctilucent clouds were detected (Fiedler et al., 2017, table 1). With respect to the focus on events with rapid altitude changes and the selection of bright NLC, a subset of ~182 h is taken into account for this study. Analyzing samples of 10 min length, this yields a number of 1094 individual measurement intervals which is sufficient to get an overview of the presence of relevant features. Only one category is assigned to every 10 min interval of NLC measurements. Thus the resolution of the calculated occurrence time of each type is no better than 10 min. The times are not weighted with the number of categorized structures or the duration of NLC detection inside this time interval. Apart from that the biggest uncertainty for the statistics is the assignment of the types by naked eye. A small degree of subjectivity can therefore not be avoided,

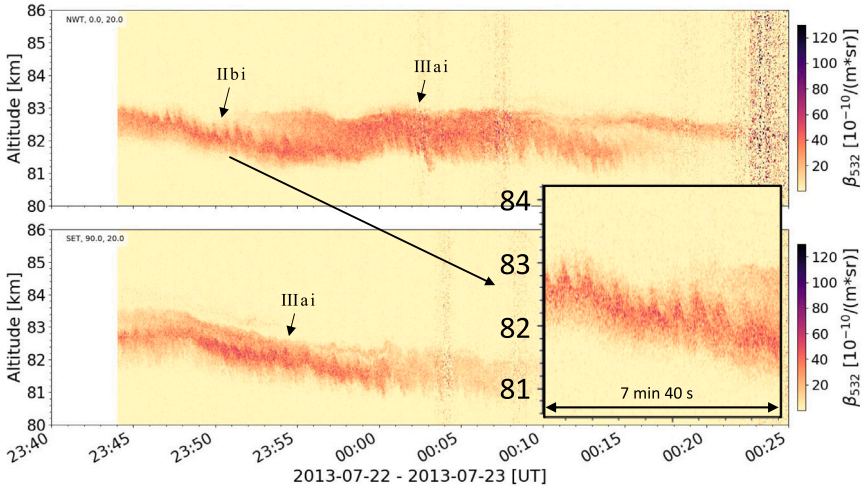

Fig. 5. Simultaneous observations on July 22, 2013 showing NLC of category II b i and III a i as labeled. The close-up shows altitude variations with short periods, mainly at the top of the layer.

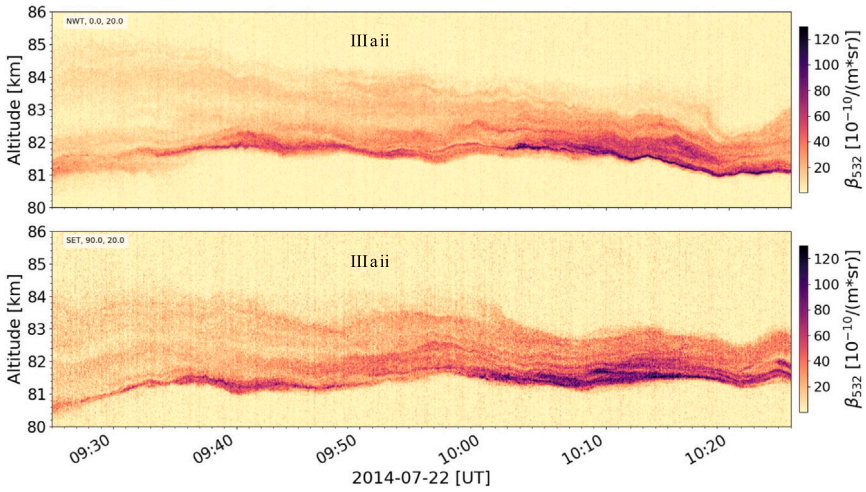

Fig. 6. Simultaneous observations of NLC on July 22, 2014 showing category III a ii. As in Fig. 4 for category II b ii, the shown case is again one with larger backscatter at the lower edge of the layer.

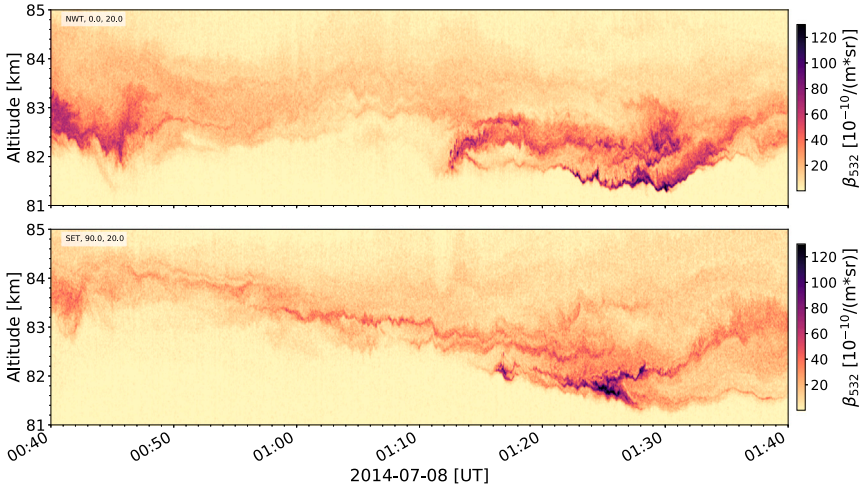

Fig. 7. Simultaneous observations of NLC on July 08, 2014 showing category III b. Here the profiles of the tilted telescopes show more differences concerning small-scale structures than in type III a ii (Fig. 6) although their spatial separation is the same.

in the choice of subcategories as well as in the decision of the layer thickness in cases with very diffuse upper and lower edges.

The histogram of the occurrence of the NLC types and categories defined in chapter 3.2 is given in Fig. 9. Here 100% refers to the

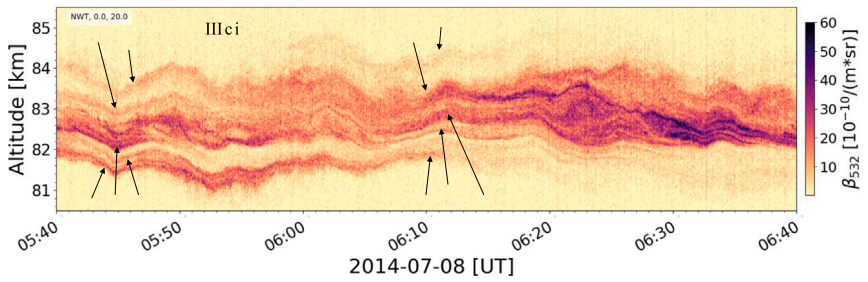

Fig. 8. NLC observation on July 08, 2014 showing category III c i. In this case up to five layers exist and move parallel at the same time (indicated by arrows). Their vertical separation is sometimes only about 100 m.

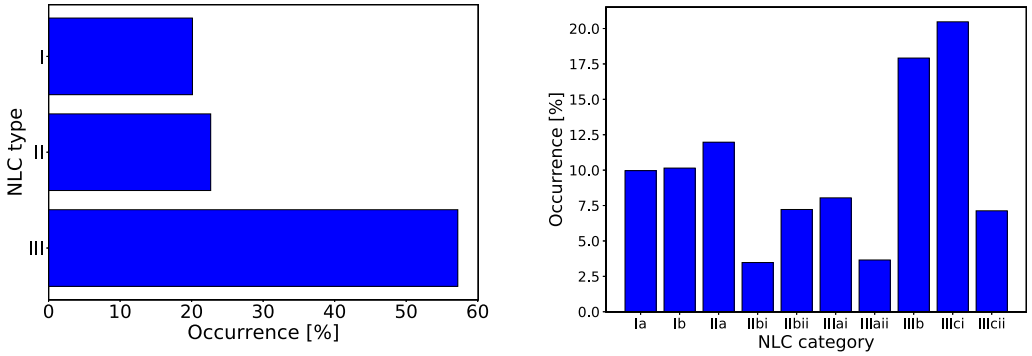

Fig. 9. Percentage of occurrence of NLC types (left) and categories (right) in lidar data from the season 2014. Types are assigned according to layer thickness (I: < 500 m, II: 500 m - 1 km, III: > 1 km), and they are subdivided into categories in order to account for short-period variations in structure (a: periods > 10 min, b: < 10 min, c: multi-layer). The total number of analyzed 10 min-intervals is 1094, i.e. 182 h of NLC measurements.

total number of 182 h analyzed in 2014. Thick layers (type III) of > 1 km thickness occur more than half of the time (57.2%), followed by middle thick layers (type II) at 22.7% and thin layers (<500 m, type I) at 20.1% of the time. Among type-I-NLC the categories a and b occur nearly equally often with a slight favor towards b (I a 10.0%, I b 10.1%). Among NLC of type II the most common category is II a, i.e. not showing short-period height variations. Concerning category II b the version with higher backscatter at the lower or upper edge of the layer (II b ii) occurs more than double as often as the vertically even distributed type II b i. Among thick layers the categories III c i and III b are dominant. Altogether, parallel moving layers (category III c i) occur with 20.5% most often of all defined categories, and it is noteworthy that the probability of multiple layers to move independently from each other (category III c ii) is with 7.1% remarkably small.

4.2. Physical interpretation

There are several questions connected to physical processes in NLC, where the occurrence statistics of certain NLC types may help to identify events of wave dissipation and turbulence generation. Microphysical processes affecting the appearance of NLC include the growth and sublimation of ice particles as well as their drift in vertical and horizontal direction. In the following a few simple calculations are made in order to explore whether certain processes can explain the formation of the different NLC types or connect them to background conditions. An interesting topic is to examine whether rapid altitude changes coincide with brightness changes and if so, how the changes are caused. The most important factor influencing the brightness is particle size, since the backscattered intensity scales with r^5 to r^6 for visible light, where r is the radius of the particle. Zasetsky et al. (2009) report on particle growth at different temperatures. Their observations show that the equilibrium sizes in a given atmospheric state vary from 25 nm at 131 K to 70 nm at 152 K. Not only the reached equilibrium sizes, but also the growth speed differs significantly with temperature. The most rapid growth is possible at 150 K with an increase in radius by 10 nm in only 20 min. This enlargement of the radius causes in turn a major increase in backscatter, e.g. ~400% for a change from 30 nm to 40 nm. It is worth noting that this correlation of temperature and growth rate is due to the increased H_2O partial pressure at lower altitudes (e.g., Kiliani et al., 2013). Thus, their result is suitable to explain rapid changes at the bottom of the layer where the highest temperatures are found. In our study, NLC altitude varies rapidly on time scales shorter than 10 min, so a constant bottom altitude and temperature are not self-evident. Therefore we shall also calculate the difference in equilibrium particle size between two positions that are vertically separated by 1 km. Assuming a typical lapse rate of −5 to −8 K/km for the upper mesosphere as reported by Lübken (1999), this temperature difference corresponds to a change in equilibrium size of at least 10 nm. That means, a vertical dislocation of a NLC layer by 1 km and letting it approach the new equilibrium state would change the brightness about as much as letting the particles grow for 20 min at a temperature of 150 K.

An example where the ice particle growth rate well explains the observed increase in brightness at the bottom of the layer is given in Fig. 6, and in more general terms it is most often suitable for events that belong to the NLC categories II a and III a. This indicates that the slower waves present here (periods > 10 min) do not effectively change the established vertical stratification of NLC brightness. On the other hand, altitude variations with periods below 10 min often do not include significant brightness changes (e.g., Fig. 3), so we do not expect the particle size to modify either. Earlier studies suggest that NLC particles can be treated as inert tracers on short time scales of a few minutes and occasionally up to one hour (Baumgarten et al., 2012), and we conclude that this is also the case for particles involved in the short-period altitude variations presented here. However, a further investigation of whether NLC behave as inert tracers requires additional

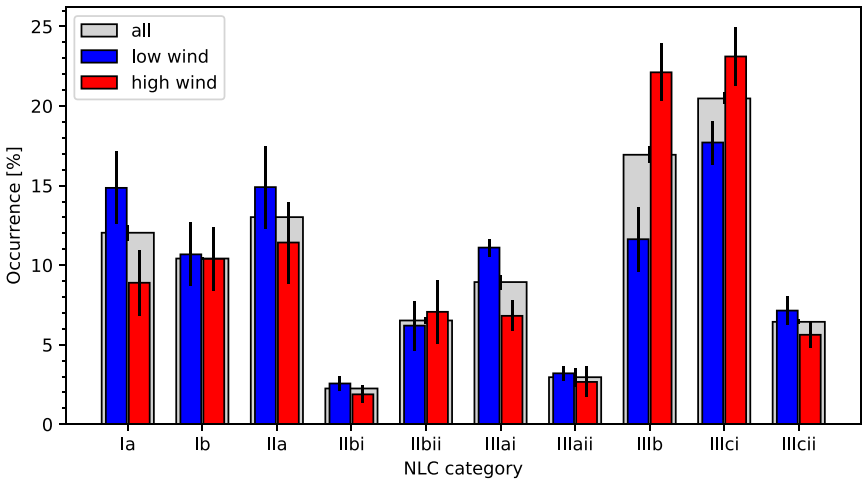

Fig. 10. Occurrence statistics for measurements where observations of horizontal wind speeds are available. The gray columns show the fractions for the total number of cases, the blue and red columns show the distribution, divided according to wind speed. The separation is at 53 m/s. The total number of observations with corresponding wind information is 874, whereof 418 belong to the low wind and 456 to the high wind regime. The error bars indicate the uncertainties.

observations that are beyond the scope of this study. Periodic structures in lidar measurements may have their origin both in wave activities above the instrument and structures being transported through the beam by advection. Wind speeds at the observed NLC altitude for the individual events of the lidar dataset may help in order to distinguish between the different processes, a first approach for that is shown in Section 4.3. Nevertheless, also frozen structures that move through the lidar beam by winds have been created by wave activities before, and therefore it is justified to use the period observed by lidar as basis for the categorization.

Apart from short-period altitude variations, the main finding of this study is the existence and persistence of very thin layers, both as single layers and inside multi-layered NLC. The occurrence statistics shows that the latter even is a very common phenomenon, since category III c i occurs most often. It is stunning that very thin layers can exist over one hour as e.g. in Fig. 3, experiencing so many rapid vertical movements and still not vanishing. Despite the mixing processes that we expect to take place in the mesopause region, thin layers occur frequently, probably supported by the higher viscosity in the mesosphere compared to conditions at the earth's surface.

4.3. Occurrence statistics divided by wind speed

In order to estimate to which extent the observed periods are influenced by advection, we divide the dataset according to horizontal wind speeds, calculated from combined measurements by the meteor radars in Andenes and Tromsø. The threshold for the selection of high and low wind speeds is set to 53 m/s which is the mean observed wind speed in NLC. For 874 out of the total 1094 cases wind information is available, whereof 418 cases belong to the low wind regime and 456 to high wind speeds > 53 m/s. The results of the modified occurrence statistics are shown in Fig. 10. To account for uncertainties arising from sorting the NLC occurrence fractions according to horizontal winds, we use wind information at 3 altitude levels (81.5 km, 82.5 km, 83.5 km) and assign the standard deviation of the classification results as error bar.

When comparing the total NLC occurrences per category in Fig. 10 (gray bars) with Fig. 9, we find slight deviations which are caused by the reduced number of observations taken into account in Fig. 10. However, the amplitude relationship between the individual categories are generally conserved.

If we assume that a given horizontal structure is purely transported by winds, we expect to see shorter periods in the lidar time series at higher wind speeds, i.e. an increase of occurrence in categories with short-period structures (mainly *b*) and a decrease in categories with wave periods > 10 min (mainly *a*). In 3 out of 4 "*a*"-categories (I a, II a, III a i) the occurrence for low wind speeds is higher compared to the one for high wind speeds, which satisfies the expectation. The fourth category (III a ii) has only about 10 low and high wind cases and may therefore be neglected. For the "*b*"-categories only III b shows the expected behavior with a distinct enhanced occurrence during high wind speeds. Categories I b and II b ii show nearly equal distributions regarding the wind speed, whereas II b i has a generally low occurrence.

In summary, part of our NLC measurements match the scenario of pure advection of the observed structures, mainly for periods > 10 min ("*a*"-categories). Interestingly, for thin layers with short periods (category I b) the picture of pure advection fails for a significant amount of cases. Hence one could conclude that such structures are not affected by advection and may be imprinted near the lidar sounding volumes.

Furthermore, advection seems to play a larger role in thicker layers and is less important in thin layers. For very short-period structures below 1 min in category III b (e.g., Fig. 7, panel 1 around 01:30 UT and panel 2 around 01:10 UT) we propose that the structures originate from earlier wave breakdown mechanisms and are then transported through the lidar beam via advection.

Despite the value of horizontal wind information for interpreting observed structures in NLC time series, a robust answer of the question whether such structures are advected by wind or generated above the lidar instrument needs additional information, like vertical winds measured at the lidar sounding volume or 2-dimensional imaging of the NLC layer surrounding of the lidar sounding volume.

5. Conclusions

Analyzing daylight lidar measurements with the unprecedented resolution of about 1 s temporally and 25 m vertically enabled the discovery of new features and insights into the dynamics of noctilucent clouds and the upper mesosphere.

1. Wave structures in noctilucent clouds are found on even shorter time scales than previously expected. Especially in cases where the data with 30 s temporal resolution looks discontinuous, in the data with 1 s resolution periodic structures are found.
2. A new categorization of NLC structures measured by lidar, focusing on small-scale structures of less than 10 min, is established and applied.

3. The formation of very thin layers (<100 m thickness), both as a single layer and inside multi-layer phenomena, is captured for the first time. Also, short vertical distances between parallel moving layers down to 100 m are observed.
4. Occurrence statistics of the newly defined NLC categories document that both small-scale wave structures and parallel moving layers are common features in NLC. The presence of structures with periods below 10 min covers more than half of the NLC measurements of type I and II in 2014 (NLC of thin and middle thickness). Multiple parallel moving layers (i.e., category III c i) have the largest frequency of occurrence of all categories.
5. Particle growth rates and background conditions are considered in order to understand structures in NLC. Inside short-period altitude variations below 10 min, brightness does not change significantly, which supports the hypothesis that ice particles are inert tracers and do not change their properties during rapid vertical displacements. Especially in thick layers, small-structure movements are most likely caused by disturbances in the flow due to wave breakdown.
6. NLC with more than 10 min period structures occur more often during low wind conditions, which supports the scenario of an advection of such structures by horizontal winds.

The observation of the presented small-scale structures in high-resolution lidar data may be used to confirm and improve model simulations of gravity wave interaction and dissipation in the mesopause region. In further studies an investigation of the occurrence of the newly defined categories depending on other variables like altitude or day of the year/season should be performed. With the categories introduced in this work an automation of the categorization is possible in order to analyze the data of more years in shorter intervals.

Acknowledgments

We are very grateful to everyone contributing to the long time series of NLC measurements at ALOMAR including IAP staff, the Norwegian ALOMAR staff and measuring students. We thank J. Chau for providing the multistatic specular meteor winds published in Chau et al. (2017). We thank Dave Fritts for the fruitful discussion.

This paper is partly supported by the TIMA project of the BMBF research initiative ROMIC and by the DFG project LU 1174/8-1 (PACOG) which is part of the research group FOR 1898 (MS-GWaves).

References

Backhouse, T.W., 1885. The luminous cirrus clouds of June and July. Meteorol. Mag. 20, 133.

Baumgarten, G., 2010. Doppler Rayleigh/mie/Raman lidar for wind and temperature measurements in the middle atmosphere up to 80 km. Atmos. Meas. Tech. 3 (6), 1509–1518. http://dx.doi.org/10.5194/amt-3-1509-2010, URL https://www.atmos-meas-tech.net/3/1509/2010/.

Baumgarten, G., Chandran, A., Fiedler, J., Hoffmann, P., Kaifler, N., Lumpe, J., Merkel, A., Randall, C.E., Rusch, D., Thomas, G., 2012. On the horizontal and temporal structure of noctilucent clouds as observed by satellite and lidar at ALOMAR (69N). Geophys. Res. Lett. 39 (1), http://dx.doi.org/10.1029/2011GL049935, URL https://agupubs.onlinelibrary.wiley.com/doi/abs/10.1029/2011GL049935.

Baumgarten, G., Fiedler, J., von Cossart, G., 2007. The size of noctilucent cloud particles above ALOMAR (69N,16E): Optical modeling and method description. Adv. Space Res. 40 (6), 772–784. http://dx.doi.org/10.1016/j.asr.2007.01.018, URL http://www.sciencedirect.com/science/article/pii/S0273117707000178.

Chau, J.L., Stober, G., Hall, C.M., Tsutsumi, M., Laskar, F.I., Hoffmann, P., 2017. Polar mesospheric horizontal divergence and relative vorticity measurements using multiple specular meteor radars. Radio Sci. 52 (7), 811–828. http://dx.doi.org/10.1002/2016RS006225.

Fiedler, J., Baumgarten, G., Berger, U., Lübken, F.-J., 2017. Long-term variations of noctilucent clouds at ALOMAR. J. Atmos. Sol.-Terr. Phys. 162, 79–89. http://dx.doi.org/10.1016/j.jastp.2016.08.006.

Fogle, B., Haurwitz, B., 1966. Noctilucent clouds. Space Sci. Rev. 6, 279. http://dx.doi.org/10.1007/BF00173768.

Fritts, D.C., Wang, L., Baumgarten, G., Miller, A.D., Geller, M.A., Jones, G., Limon, M., Chapman, D., Didier, J., Kjellstrand, C.B., Araujo, D., Hillbrand, S., Korotkov, A., Tucker, G., Vinokurov, J., 2017. High-resolution observations and modeling of turbulence sources, structures, and intensities in the upper mesosphere. J. Atmos. Sol.-Terr. Phys. 162, 57–78. http://dx.doi.org/10.1016/j.jastp.2016.11.006, Layered Phenomena in the Mesopause Region, URL http://www.sciencedirect.com/science/article/pii/S1364682616304126.

Hall, C.M., Aso, T., Tsutsumi, M., Nozawa, S., Manson, A.H., Meek, C.E., 2005. A comparison of mesosphere and lower thermosphere neutral winds as determined by meteor and medium-frequency radar at 70°N. Radio Sci. 40 (4), n/a–n/a. http://dx.doi.org/10.1029/2004rs003102.

Jesse, O., 1885. Auffallende Abenderscheinungen am Himmel. Meteorol. Z. 2, 311–312.

Kaifler, N., Baumgarten, G., Fiedler, J., Latteck, R., Lübken, F.-J., Rapp, M., 2011. Coincident measurements of PMSE and NLC above ALOMAR (69° N, 16° E) by radar and lidar from 1999–2008. Atmos. Chem. Phys. 11 (4), 1355–1366. http://dx.doi.org/10.5194/acp-11-1355-2011, URL https://www.atmos-chem-phys.net/11/1355/2011/.

Kaifler, N., Baumgarten, G., Fiedler, J., Lübken, F.-J., 2013. Quantification of waves in lidar observations of noctilucent clouds at scales from seconds to minutes. Atmos. Chem. Phys. 13 (23), 11757–11768. http://dx.doi.org/10.5194/acp-13-11757-2013, URL https://www.atmos-chem-phys.net/13/11757/2013/.

Karlsson, B., Rapp, M., 2006. Latitudinal dependence of noctilucent cloud growth. Geophys. Res. Lett. 33 (11), http://dx.doi.org/10.1029/2006GL025805, URL https://agupubs.onlinelibrary.wiley.com/doi/abs/10.1029/2006GL025805.

Kiliani, J., Baumgarten, G., Lübken, F.-J., Berger, U., Hoffmann, P., 2013. Temporal and spatial characteristics of the formation of strong noctilucent clouds. J. Atmos. Sol.-Terr. Phys. 104, 151–166.

Leslie, R.C., 1885. Sky glows. Nature 32, 245, URL https://doi.org/10.1038/032245a0.

Lübken, F.-J., 1999. Thermal structure of the arctic summer mesosphere. J. Geophys. Res.: Atmos. 104 (D8), 9135–9149. http://dx.doi.org/10.1029/1999JD900076, URL https://agupubs.onlinelibrary.wiley.com/doi/abs/10.1029/1999JD900076.

Lübken, F.-J., Berger, U., Baumgarten, G., 2018. On the anthropogenic impact on long-term evolution of noctilucent clouds. 45, Geophys. Res. Lett. 45.http://dx.doi.org/10.1029/2018GL077719,

Nussbaumer, V., Fricke, K.H., Langer, M., Singer, W., von Zahn, U., 1996. First simultaneous and common volume observations of noctilucent clouds and polar mesosphere summer echoes by lidar and radar. J. Geophys. Res.: Atmos. 101 (D14), 19161–19167. http://dx.doi.org/10.1029/96JD01213, URL https://agupubs.onlinelibrary.wiley.com/doi/abs/10.1029/96JD01213.

Picone, J.M., Hedin, A.E., Drob, D.P., Aikin, A.C., 2002. NRLMSISE-00 empirical model of the atmosphere: Statistical comparisons and scientific issues. J. Geophys. Res.: Space Phys. 107 (A12), SIA 15–1–SIA 15–16. http://dx.doi.org/10.1029/2002JA009430, URL https://agupubs.onlinelibrary.wiley.com/doi/abs/10.1029/2002JA009430.

Ridder, C., Baumgarten, G., Fiedler, J., Lübken, F.-J., Stober, G., 2017. Analysis of small-scale structures in lidar observations of noctilucent clouds using a pattern recognition method. J. Atmos. Sol.-Terr. Phys. 162, 48–56. http://dx.doi.org/10.1016/j.jastp.2017.04.005, URL http://www.sciencedirect.com/science/article/pii/S1364682617302535. Layered Phenomena in the Mesopause Region.

Singer, W., von Zahn, U., Weiß, J., 2004. Diurnal and annual variations of meteor rates at the arctic circle. Atmos. Chem. Phys. 4 (5), 1355–1363. http://dx.doi.org/10.5194/acp-4-1355-2004.

Thomas, G.E., Olivero, J.J., Jensen, E.J., Schroeder, W., Toon, O.B., 1989. Relation between increasing methane and the presence of ice clouds at the mesopause. Nature 338, 490–492. http://dx.doi.org/10.1038/338490a0.

Turco, R., Toon, O., Whitten, R., Keesee, R., Hollenbach, D., 1982. Noctilucent clouds: Simulation studies of their genesis, properties and global influences. Planet. Space Sci. 30 (11), 1147–1181. http://dx.doi.org/10.1016/0032-0633(82)90126-X, URL http://www.sciencedirect.com/science/article/pii/003206338290126X.

von Zahn, U., von Cossart, G., Fiedler, J., Fricke, K.H., Nelke, G., Baumgarten, G., Rees, D., Hauchecorne, A., Adolfsen, K., 2000. The ALOMAR Rayleigh/mie/Raman lidar: objectives, configuration, and performance. Ann. Geophys. 18, 815–833. http://dx.doi.org/10.1007/s00585-000-0815-2.

Zasetsky, A.Y., Petelina, S.V., Remorov, R., Boone, C.D., Bernath, P.F., Llewellyn, E.J., 2009. Ice particle growth in the polar summer mesosphere: Formation time and equilibrium size. Geophys. Res. Lett. 36 (15), n/a–n/a. http://dx.doi.org/10.1029/2009GL038727, L15803.